Molecular Biology of the Cell
Vol. 18, 3144–3155, August 2007

# Myosin-IIA Heavy-Chain Phosphorylation Regulates the Motility of MDA-MB-231 Carcinoma Cells

**Natalya G. Dulyaninova,* Reniqua P. House,* Venkaiah Betapudi,† and Anne R. Bresnick***

*Department of Biochemistry, Albert Einstein College of Medicine, Bronx, NY 10461; and †Department of Physiology and Biophysics, Case Western Reserve University, Cleveland, OH 44106-4970

Submitted November 30, 2006; Revised May 30, 2007; Accepted June 1, 2007
Monitoring Editor: Yu-li Wang

**In mammalian nonmuscle cells, the mechanisms controlling the localized formation of myosin-II filaments are not well defined. To investigate the mechanisms mediating filament assembly and disassembly during generalized motility and chemotaxis, we examined the EGF-dependent phosphorylation of the myosin-IIA heavy chain in human breast cancer cells. EGF stimulation of MDA-MB-231 cells resulted in transient increases in both the assembly and phosphorylation of the myosin-IIA heavy chains. In EGF-stimulated cells, the myosin-IIA heavy chain is phosphorylated on the casein kinase 2 site (S1943). Cells expressing green fluorescent protein-myosin-IIA heavy-chain S1943E and S1943D mutants displayed increased migration into a wound and enhanced EGF-stimulated lamellipod extension compared with cells expressing wild-type myosin-IIA. In contrast, cells expressing the S1943A mutant exhibited reduced migration and lamellipod extension. These observations support a direct role for myosin-IIA heavy-chain phosphorylation in mediating motility and chemotaxis.**

## INTRODUCTION

Enhanced migration is a fundamental characteristic of tumor cells and is thought to contribute to invasion and metastasis. Acquisition of a migratory state together with the loss of cell–cell adhesions allows cancer cells to detach from the primary tumor and transverse surrounding blood or lymphatic vessels (Chambers *et al.,* 2002). Chemotactic migration contributes to the metastatic process; however, the mechanisms that mediate the complex interplay of cytoskeletal rearrangement and extracellular matrix interactions are not fully understood (Yamaguchi *et al.,* 2005). Direct motility involves protrusive activity at the leading edge of the cell and adhesion of the leading lamellipod to extracellular matrix components. These events are followed by the development of contractile force that permits the detachment of focal contacts at the rear of the cell, and retraction of the tail toward the leading lamella. Although recent studies implicate type II myosin in both posterior tail retraction and anterior protrusion (Lo *et al.,* 2004; Betapudi *et al.,* 2006; Kolega, 2006), the regulatory mechanisms mediating myosin-II function during cytoskeletal remodeling have not been identified.

Nonmuscle myosin-II is a hexameric complex comprised of two heavy chains (NMHC-II), two essential light chains, and two regulatory light chains (Bresnick, 1999). In vertebrates, there are three NMHC-II isoforms (NMHC-IIA, NMHC-IIB, and NMHC-IIC), which exhibit distinct patterns of expression that are tissue and cell type dependent (Golomb *et al.,* 2004). Despite a high level of conservation, the NMHC-II isoforms have different enzymatic activities (Kovacs *et al.,* 2003; Rosenfeld *et al.,* 2003; Wang *et al.,* 2003), exhibit distinct patterns of localization within a single cell type (Maupin *et al.,* 1994; Kolega, 1998), and interact with different proteins (Kriajevska *et al.,* 1994; Huang *et al.,* 2003; Obungu *et al.,* 2003; Clark *et al.,* 2006), suggesting that the isoforms have unique functional roles in vivo. This idea is supported by gene disruption and cell biological studies demonstrating that for many cellular processes, the NMHC-II isoforms cannot compensate for one another (Tullio *et al.,* 1997; Conti *et al.,* 2004; Lo *et al.,* 2004; Meshel *et al.,* 2005; Cai *et al.,* 2006; Jana *et al.,* 2006).

In mammalian cells, phosphorylation on Ser-19 of the myosin-II regulatory light chain is a commonly invoked mechanism for the regulation of assembly in vivo, as in vitro studies demonstrate that light chain phosphorylation promotes filament assembly (Scholey *et al.,* 1980). However, there is considerable biochemical evidence for the regulation of nonmuscle myosin-II assembly via heavy-chain phosphorylation. Specifically, heavy-chain phosphorylation by protein kinase C (PKC) and casein kinase 2 (CK2) has been characterized for myosin-IIA and IIB. PKC phosphorylates NMHC-IIA on Ser1916, which is near the C-terminal end of the coiled-coil, and myosin-IIB on multiple serines in the tailpiece (Conti *et al.,* 1991; Murakami *et al.,* 1998). CK2 phosphorylates NMHC-IIA on Ser1943 in the tailpiece and NMHC-IIB on several serines in the tailpiece (Murakami *et al.,* 1998). Heavy-chain phosphorylation by either PKC or CK2 reduces the assembly of both myosin-II isoforms into filaments (Murakami *et al.,* 1995; Murakami *et al.,* 1998; Dulyaninova *et al.,* 2005).

This article was published online ahead of print in *MBC in Press* (http://www.molbiolcell.org/cgi/doi/10.1091/mbc.E06–11–1056) on June 13, 2007.

Address correspondence to: Anne R. Bresnick (bresnick@aecom.yu.edu).

Abbreviations used: NMHC-IIA, nonmuscle myosin-IIA heavy chain; NMHC-IIB, nonmuscle myosin-IIB heavy chain; RLC, regulatory light chain; GFP, green fluorescent protein; CK2, casein kinase 2; PKC, protein kinase C.

In addition to phosphorylation, myosin-IIA assembly is regulated via the binding of the metastasis factor, mts1 or S100A4 (Garrett *et al.*, 2006). S100A4 preferentially binds to nonmuscle myosin-IIA in a $Ca^{2+}$-dependent manner and promotes the monomeric, unassembled state of myosin-IIA (Li *et al.*, 2003). Phosphorylation on Ser1943 of the NMHC-IIA by CK2 inhibits S100A4 binding and protects against S100A4-induced inhibition of filament assembly and S100A4-mediated depolymerization of myosin-IIA filaments (Li *et al.*, 2003; Dulyaninova *et al.*, 2005). Thus heavy-chain phosphorylation and $Ca^{2+}$ binding regulate the S100A4/myosin-IIA interaction.

To examine the mechanisms controlling myosin-IIA assembly that contribute to the motility of breast carcinoma cells, we evaluated the contribution of NMHC-IIA phosphorylation to the chemotactic response of human breast cancer cells. Our studies show that EGF stimulation of MDA-MB-231 cells results in phosphorylation of the NMHC-IIA on the CK2 site (S1943). Expression of NMHC-IIA mutants that mimic constitutively phosphorylated or nonphosphorylatable analogs of the NMHC-IIA affects cell migration into a wound, EGF-stimulated lamellipod extension, and turnover of focal adhesion structures. These observations support a direct role for NMHC-IIA phosphorylation in mediating cell motility and chemotaxis.

## MATERIALS AND METHODS

### *Myosin-IIA Constructs*

pTRE-GFP-NMHC-IIA (Wei and Adelstein, 2000) containing the corrected human full-length nonmuscle myosin-IIA heavy chain was a gift from Dr. Robert Adelstein (National Heart, Lung, and Blood Institute, Bethesda, MD) and Dr. Thomas Egelhoff (Case Western Reserve University, Cleveland, OH). Inconsistencies in the human NMHC-IIA sequence were resolved recently. The corrected NMHC-IIA encodes a protein 1960 residues in length and the numbering used in this article reflects the corrected sequence. Our previously published work used the numbering from an older version of the NMHC-IIA sequence (1961 residues). A DNA fragment encoding residues 1–1960 from nonmuscle myosin-IIA heavy chain was subcloned into the HindIII and SalI sites of pEGFP-C3 (Clontech, Palo Alto, CA) and will be referred to as green fluorescent protein (GFP)-NMHC-IIA hereafter. Using the Quick Change XL site-directed mutagenesis kit (Stratagene, La Jolla, CA), Ser1943 was substituted with alanine, aspartic, or glutamic acid in both the full-length GFP-NMHC-IIA and myosin-IIA rods (Li *et al.*, 2003). All constructs were confirmed by DNA sequencing. mCherry was PCR-amplified from pRSET-Bm (Shaner *et al.*, 2004) and cloned into the AgeI and HindIII sites of pEGFP-NMHC-IIA-C3 to create the pmCherry-NMHC-IIA expression vector.

### *Cell Culture*

The MDA-MB-231 human breast cancer cell line was obtained from the American Type Culture Collection (Manassas, VA) and maintained as monolayer cultures in DMEM supplemented with 10% fetal bovine serum (FBS) at 37°C with 5% $CO_2$. For $^{32}P$-labeling, MDA-MB-231 cells were plated at 40–50% confluence. After ~20 h, the medium was replaced with phosphate-free DMEM. After 30 min, the phosphate-free medium was replaced with phosphate-free medium containing 0.5% FBS and 200 $\mu$Ci/ml [$^{32}P$]orthophosphate (NEN Life Sciences, Boston, MA). After 14–16 h of radiolabeling, mitotic cells were removed by selective detachment and the attached cells were stimulated with 30 ng/ml EGF (Invitrogen, Carlsbad, CA) for 0–20 min. For phosphoamino acid and phosphopeptide mapping studies, MDA-MB-231 cells were starved and radiolabeled overnight in phosphate-free DMEM containing 0.5% FBS and 330 $\mu$Ci/ml [$^{32}P$]orthophosphate and stimulated with 30 ng/ml EGF for 3 min.

### *Transfections*

Wild-type GFP-NMHC-IIA or S1943 mutants were introduced into MDA-MB-231 cells by electroporation (Amaxa Biosystems, Gaithersburg, MD). Stable MDA-MB-231 transfectants were generated by selection in 800 $\mu$g/ml G418 (Invitrogen) and could be maintained in culture with 400 $\mu$g/ml G418 for approximately 1 mo before they began to lose fluorescence. TransIT-HelaMONSTR reagent (Mirus, Madison, WI) was used for transient tranfections after careful optimization of transfection parameters. Cells were examined in lamellipod extension assays and immunofluorescence studies 24–48 h after transfection as described below.

### *Antibodies*

Affinity-purified, rabbit polyclonal antibodies to the C-termini of myosin-IIA and myosin-IIB were generated as described previously (Li and Bresnick, 2006). A polyclonal antibody directed against the alpha subunit of CK2 was kindly provided by Dr. U. Thomas Meier (Albert Einstein College of Medicine, Bronx, NY; Litchfield *et al.*, 1994). Paxillin and phosphospecific paxillin pY118 antibodies were from Chemicon International (Temecula, CA) and Biosource (Camarillo, CA; cat 44–722), respectively. The $\beta$-actin and vinculin antibodies were purchased from Sigma (St. Louis, MO). Phospho-regulatory light chain (RLC) antibodies (T18/S19 and S19) were purchased from Cell Signaling Technology (Beverly, MA).

### *Immunoprecipitation*

For immunoprecipitation of the endogenous myosin-II heavy chains, $^{32}P$-labeled and EGF-stimulated cells were washed three times with ice-cold phosphate-buffered saline (PBS) and resuspended in lysis buffer composed of 50 mM Tris-HCl, pH 7.4, 400 mM NaCl, 1% NP-40, 2.5 mM EGTA, 10 mM $MgCl_2$, 1 mM DTT, 1 mM PMSF, 5 $\mu$g/ml each of chymostatin, leupeptin, pepstatin A, and a 1:100 dilution of phosphatase inhibitor cocktail I (microcystine LR, cantharidin, and (−)-*p*-bromotetramisole) and phosphatase inhibitor cocktail II (sodium vanadate, sodium molybdate, sodium tartrate, and imidazole; Sigma). The cell extracts were incubated on ice for 20 min, and the lysate was clarified by centrifugation at 4°C for 15 min at 14,000 × *g*. The supernatant was diluted 1:1 in 20 mM Tris-HCl, pH 7.4, 2.5 mM EGTA, 1 mM dithiothreitol (DTT), 1 mM phenylmethylsulfonyl fluoride (PMSF) with protease and phosphatase inhibitors as described above. Before the immunoprecipitation, rabbit polyclonal antibodies to the C-termini of myosin-IIA and myosin-IIB were bound to protein A-Sepharose (Sigma) in PBS containing 1 mg/ml bovine serum albumin (BSA). The diluted supernatant was incubated with the antibody-protein A-Sepharose at 4°C for 2 h. Immune complexes were collected by centrifugation and washed five times with 20 mM Tris-HCl, pH 7.4, 150 mM NaCl, 0.5 mM DTT. Laemmli sample buffer, 2× (Laemmli, 1970), was added to the immune complexes, which were boiled, and the proteins were separated by 6% SDS-PAGE or 12% Tris-Tricine SDS-PAGE to visualize the myosin heavy chain (MHC) or RLC, respectively. $^{32}P$-labeled myosin-IIA was visualized by autoradiography of the dried gel. Relative phosphorylation of the myosin-IIA heavy chain was determined by dividing the values obtained from autoradiography by the values obtained from densitometry of Coomassie-stained gels.

### *Stoichiometry of Phosphorylation*

To determine the moles of phosphate incorporated per mole NMHC-IIA, the specific activity of cellular ATP pools in MDA-MB-231 cells was measured using the $^{32}P$ labeling conditions described above. Extraction of $^{32}P$-labeled ATP from cell lysates was performed by precipitation with cold 12% trichloroacetic acid. Aliquots of the supernatant were applied to a PEI-cellulose TLC plate followed by chromatography in phosphate solution as described previously (Cashel *et al.*, 1969). [32P]ATP was visualized by autoradiography and quantified using Cerenkov counting. To determine total cellular ATP, cell extracts were diluted 40 times with distilled water, and the ATP concentration was quantified using a bioluminescent ATP determination kit (Sigma). The specific activity of the cellular ATP in MDA-MB-231 cells (3852 ± 240 cpm/pmol ATP) was used to calculate the moles of phosphate incorporated into the myosin-IIA heavy and light chains. Cells were lysed as described above, and myosin-IIA was immunoprecipitated from cell supernatants. The moles of NMHC-IIA in immunoprecipitates from 0 and 3 min after EGF stimulation was determined by densitometry of Coomassie-stained gels and comparison to a standard curve of purified myosin-II heavy chain.

### *Phosphoamino Acid Analysis and Phosphopeptide Mapping*

Two-dimensional phosphopeptide mapping and phosphoamino acid analyses were performed using standard methods. Briefly, immunoprecipitates of $^{32}P$-labeled endogenous myosin-IIA heavy chains or in vitro PKC or CK2-phosphorylated myosin-IIA rods were subjected to SDS-PAGE and transferred to Hybond nitrocellulose membrane (Amersham Pharmacia Biotech, Piscataway, NJ). The membrane was stained with Ponceau S and autoradiographed, and $^{32}P$-labeled protein bands were excised and blocked for 30 min at 37°C in 0.5% PVP-40 in 100 mM acetic acid. Tryptic digests and phosphoamino analysis and two-dimensional phosphopeptide mapping were performed as described previously (Dulyaninova *et al.*, 2004).

### *Immunoblots*

Triton-insoluble fractions of EGF-stimulated MDA-MB-231 cells were prepared by lysis in ice-cold Triton X-100 (Tx-100 buffer; 50 mM Tris-HCl pH 7.4, 100 mM NaCl, 50 mM KCl, 5 mM $MgCl_2$, 0.5% Tx-100, 5 mM DTT, 1 mM PMSF with protease and phosphatase inhibitors as described above). After 5 min of incubation, soluble and insoluble proteins were separated by centrifugation and Triton-insoluble components were resuspended in 2× Laemmli sample buffer. To confirm expression of the full-length GFP-MIIA wild-type and S1943 mutants in MDA-MB-231 cells, whole cell lysates were prepared by placing monolayers of stable transfectants on dry ice for 10 min and then

scraping the cells into 2× Laemmli sample buffer, containing 5 μg/ml each of chymostatin, leupeptin, and pepstatin. Triton-insoluble fractions and total cell extracts were separated on 6% SDS-PAGE, followed by immunoblotting with rabbit polyclonal antibodies to the C-termini of myosin-IIA or myosin-IIB. The relative amount of cytoskeletal myosin-IIA was estimated by densitometry using ImageQuant version 5.0 (Molecular Dynamics, Sunnyvale, CA).

For immunoblots with phospho-RLC antibodies (T18/S19 or S19), total cell lysates from EGF stimulated cells were prepared by direct addition of ice-cold 10% trichloroacetic acid supplemented with 10 mM DTT to the cell culture dish. Cell samples were collected by scraping followed by microcentrifugation. Cell pellets were washed twice with ice-cold acetone containing 10 mM DTT, air-dried, resuspended in 2× Laemmli sample buffer, sonicated, boiled, and separated on 15% SDS-PAGE. To normalize for sample loading, the PVDF membrane was also reacted with a monoclonal actin antibody, and the relative phosphorylation of the RLC was estimated by densitometry as described above.

### *Myosin-IIA Biochemical Assays*

Recombinant human S100A4 was purified as described previously (Vallely *et al.*, 2002). Recombinant His-tagged human wild-type myosin-IIA rods (residues 1339–1961), and S1943 mutants were purified as described by Li *et al.* (2003). The assembly properties of the myosin-IIA rods and the effect of S1943 substitution on S100A4 binding were characterized in vitro in the presence of magnesium as described in Dulyaninova *et al.* (2005). The amount of polymerized myosin-IIA rods in assembly assays was quantified using the program ImageQuant version 5.0 (Molecular Dynamics). The solubility data were plotted as a function of NaCl concentration and fit to the Hill equation in order to compare the midpoint of the curves for wild-type and S1943 mutant rods. For S100A4 binding assays, the equilibrium binding constant was estimated by a nonlinear least squares fit using an equation that takes into account ligand depletion, $MR = [0.5(K_d + R_{tot} + M_{tot}) \pm [(-(K_d + R_{tot} + M_{tot}))^2 - 4(M_{tot})(R_{tot})]^{1/2}]$, where MR = [S100A4·myosin-II complex], $R_{tot}$ = [total myosin-II] and $M_{tot}$ = [total S100A4] (Hulme and Birdsall, 1992). For phosphopeptide mapping and phosphoamino acid analyses, stoichiometrically PKC-phosphorylated or CK2-phosphorylated myosin-IIA rods were prepared as described previously (Dulyaninova *et al.*, 2005).

To examine the interaction of CK2 with myosin-IIA, $Ni^{2+}$-agarose containing bound recombinant His-tagged myosin-IIA rods was incubated with cell lysates at 4°C. To prepare cell lysates, serum-starved MDA-MB-231 cells were stimulated with EGF for 3 min and lysed in 50 mM Tris-HCl, pH 7.4, 400 mM NaCl, 1% NP-40, 0.5 mM EGTA, 10 mM $MgCl_2$, 20 mM β-mercaptoethanol, 5% glycerol, and 1 mM PMSF with protease and phosphatase inhibitors as described above. Unstimulated cells were used as a control. After 20 min on ice, the lysate was clarified by centrifugation at 4°C for 20 min at 14,000 × *g*. Binding was performed in the presence of 40 mM imidazole. After incubation, the resin was washed five times with wash buffer containing 50 mM imidazole, 50 mM Tris-HCl, pH 7.5, 500 mM NaCl, and 20 mM β-mercaptoethanol. The bound proteins were subjected to 12% SDS-PAGE followed by immunoblotting with CK2α polyclonal antibodies.

### *Fluorescence Microscopy*

To examine the distribution of the myosin-II isoforms in cells under normal growth conditions, MDA-MB-231 cells were fixed in freshly prepared 3.7% formaldehyde in PBS for 15 min and permeabilized with 0.5% Tx-100 in fix. To examine the distribution of myosin-IIA and myosin-IIB in EGF-stimulated MDA-MB-231 cells, starved cells on Matrigel-coated cover slips (0.8 μg/cm$^2$) were stimulated for various times and then fixed for 10 min in 3.7% formaldehyde in cytoskeleton stabilization buffer (137 mM NaCl, 5 mM KCl, 1.1 mM $Na_2HPO_4$, 0.4 mM $KH_2PO_4$, 2 mM $MgCl_2$, 2 mM EGTA, 5 mM PIPES, and 5.5 mM glucose, pH 6.1; Small, 1981). The cells were permeabilized with 0.5% Tx-100 in stabilization buffer. Cells were reacted with affinity-purified, directly labeled myosin-IIA and myosin-IIB polyclonal antibodies. The NMHC-IIA polyclonal antibodies (pAb) was directly labeled with Alexa Fluor 488, and the NMHC-IIB pAb was directly labeled with Alexa Fluor 555. The directly labeled NMHC-IIB antibody exhibits some nonspecific staining of the nucleus. Coverslips were mounted in ProLong Antifade (Molecular Probes, Eugene, OR). For fluorescence microscopy of the wild-type GFP-NMHC-IIA or S1943 mutants, transfected MDA-MB-231 cells were fixed in freshly prepared 3.7% formaldehyde in PBS.

To examine the colocalization of wild-type GFP-NMHC-IIA or S1943 mutants with wild-type mCherry-NMHC-IIA, MDA-MB-231 cells were cotransfected with the two plasmids. At 24 h after transfection cells were plated on Matrigel coated–coverslips, starved, EGF-stimulated for 4–6 min, and then fixed as described above. Colocalization was analyzed in two to five fields per cell using the ImageJ plugin JACoP (Bolte and Cordelieres, 2006). A total of seven S1943A GFP-NMHC-IIA expressing cells (total of 28 fields), nine S1943D GFP-NMHC-IIA expressing cells (total of 25 fields), and seven wild-type GFP-NMHC-IIA–expressing cells (total of 26 fields) were analyzed. The Pearson's coefficient was expressed as the mean and the SD.

Immunofluorescence and NMHC-IIA colocalization images were acquired with a PlanApo 60×, 1.4 NA objective (Olympus, Melville, NY) and HiQ bandpass filters (Chroma Technology, Brattleboro, VT). For wound healing and lamellipod extension assays, images were recorded using UPlanFl 10×, 0.3 NA and UPlanFl 20×, 0.5 NA objectives, respectively. All images were acquired using IPLab Spectrum software (Scanalytics, Billerica, MA) and a CoolSNAP HQ interline 12-bit, cooled CCD camera (Roper Scientific, Tucson, AZ) mounted on an Olympus IX70 microscope. Images were processed using Photoshop (Adobe Systems, San Jose, CA) or NIH Image.

### *Cell Assays*

Cell motility was measured in a wound migration assay. Stable transfectants expressing the wild-type or S1943 GFP-NMHC-IIA mutants were grown to confluency on culture plates and a wound was made in the monolayer with a sterile P200 pipette tip (~0.5 mm in width). After wounding, the medium and debris were removed, plates were washed with PBS, and fresh medium was added. Phase-contrast images of the wound area were taken just after wounding, and the wound area was imaged at different times over a 48-h period. Wound widths were measured at a minimum of four different points for each wound, and the average rate of wound closure during the first 4 h of wound healing was calculated. If wound edges were not uniform, the average width of the wound was measured for a given field.

Adhesion of stable MDA-MB-231 transfectants was assessed in a trypsinization assay. Cells stably expressing wild-type GFP-NMHC-IIA or S1943 mutants were seeded overnight on 35-mm dishes in triplicate. Cells were treated with 400 μl of trypsin-EDTA (Invitrogen) for 1 min, and then 400 μl of cell culture medium was added to each plate followed by gentle rotation of the plate for 1 min. Detached cells were collected after the addition of another 400 μl of cell culture medium and 30 s of shaking. 400 μl of trypsin-EDTA was added to the remaining cells until all the cells were detached, and the second fraction of cells was harvested with an additional 800 μl of cell culture medium. Absorbance at 600 nm was determined for both cell fractions, and the adhesion index was determined by calculating the percentage of total cells that detached in response to the initial trypsin treatment.

Lamellipod extension of transfected cells was evaluated as the overall increase in the total area of the cells after EGF stimulation (Segall *et al.*, 1996). Cells plated on a Matrigel-coated 35-mm MatTek dish were starved overnight in DMEM containing 0.5% FBS for ~16 h. Before stimulation, the medium was replaced with Leibovitz's L15 containing 0.5% FBS, and cells were stimulated with 15 ng/ml EGF. Phase-contrast images were recorded every 20 s for 15 min with a 20× objective and 1.5× magnification, and the cells were maintained at 37°C for the duration of the experiment. The movies were assembled using NIH Image, and individual cells were traced manually. The area before stimulation was set as 100%, and the relative area change was calculated as a percentage of the initial cell area.

Unpaired Student's *t* tests were performed to assess statistical significance for all three assays.

## RESULTS

### *Transient Phosphorylation and Assembly of the Myosin-II Heavy Chain Occurs in Response to EGF Stimulation*

The regulation of myosin-II assembly has been studied extensively in lower eukaryotes (Egelhoff *et al.*, 1993; Brzeska and Korn, 1996); however, there have been few studies examining the regulatory mechanisms modulating myosin-II assembly in mammalian cells. To investigate the mechanisms controlling filament assembly and disassembly during generalized motility and chemotaxis in higher eukaryotes, we examined the EGF-dependent phosphorylation of the myosin-II heavy chains in the human breast cancer cell line, MDA-MB-231. These cells express both the A and B isoforms of nonmuscle myosin-II, but not myosin-IIC (Betapudi *et al.*, 2006). For myosin-IIA, we observed two peaks of Triton-insoluble (e.g., assembled) myosin-IIA at 1.5 and 6 min after EGF stimulation (Figures 1, A and B). We also detected two peaks for myosin-IIB assembly, with the first peak occurring at 2 min and a broader, second peak occurring at 6 min after EGF stimulation (Figure 1C). EGF stimulation of MDA-MB-231 cells resulted in a transient increase in phosphorylation of both myosin heavy-chain isoforms. The peak of NMHC-IIA phosphorylation occurred 2–3 min after EGF stimulation, with approximately a 35% increase in the extent of phosphorylation as compared with unstimulated cells (Figure 1B). For NMHC-IIB, the peak of phosphorylation was broader and peaked at ~4–6 min after stimulation with approximately a 40% increase in the extent of phosphate incorporation (Figure 1C). The kinetics of

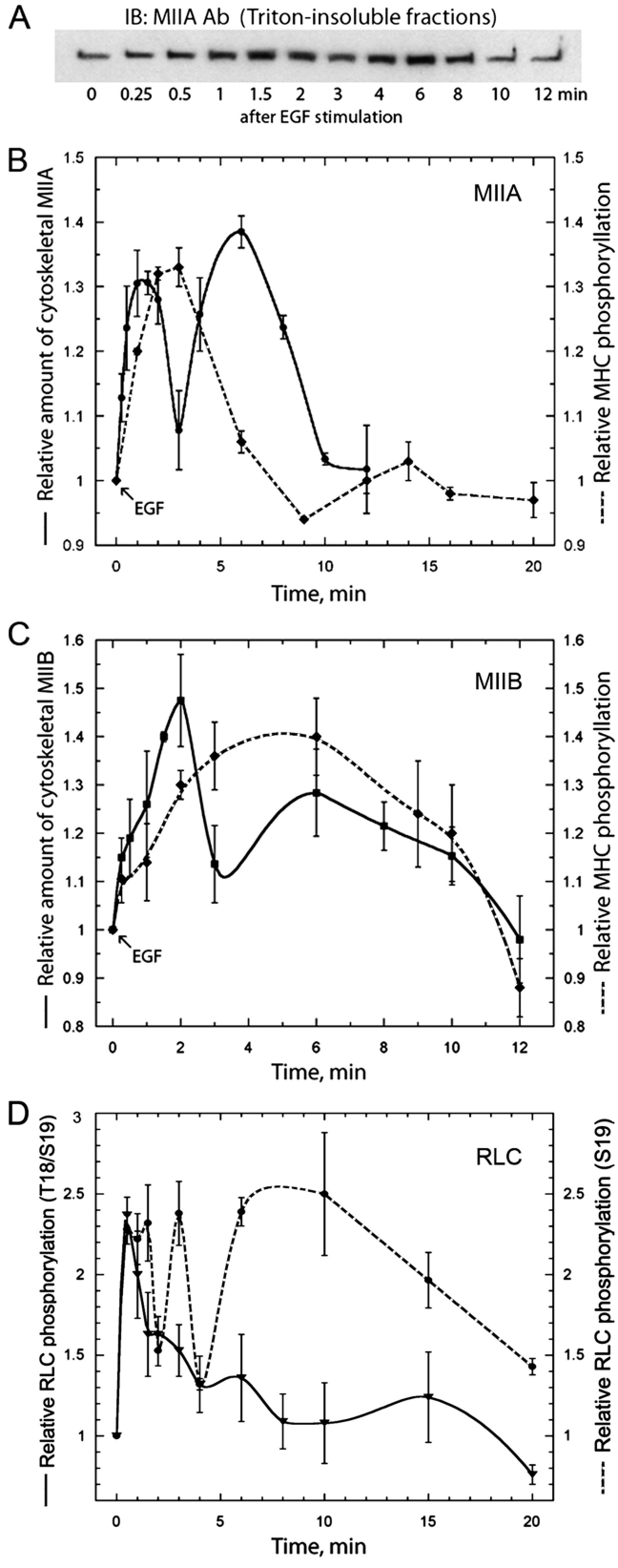


**Figure 1.** EGF stimulation of MDA-MB-231 cells resulted in transient increases in both the insolubility and phosphorylation of the myosin-II heavy chain isoforms. (A) Representative immunoblot of myosin-IIA in Triton-insoluble fractions at different times after stimulation with EGF. EGF-mediated increases in (B) myosin-IIA and (C) myosin-IIB insolubility and heavy-chain phosphorylation. Myosin-II assembly was assessed by isolating Tx-100–resistant cytoskeletons from EGF-stimulated cells. To examine the phosphorylation status on the myosin-II heavy chain, cells were serum-starved, metabolically labeled with $^{32}$P-orthophosphate, and stimulated with EGF. At different times after stimulation, the myosin-II heavy chain isoforms were immunoprecipitated and analyzed by SDS-PAGE and autoradiography. (D) EGF-mediated increases in total T18/S19 (solid line) or S19 (dotted line) RLC phosphorylation. Cells were serum-starved and stimulated with EGF. The phosphorylation status of the RLC in whole cell lysates was examined by immunoblot with P-T18/S19 and P-S19 antibodies. For all curves, values represent the mean and SE of the mean for three to four independent experiments.

NMHC-IIB assembly and phosphorylation that we observed in MDA-MB-231 cells are comparable to what has been observed previously in TSU-Pr1 cells (Straussman *et al.*, 2001; Ben-Ya'acov and Ravid, 2003). We also examined the phosphorylation status of total RLC in EGF-stimulated cells (Figure 1D). A single peak of RLC T18/S19 phosphorylation was detected at 30 s after EGF stimulation with approximately a 140% increase in phosphate incorporation. Interestingly, the kinetics of S19 phosphorylation differed from that of T18/S19 phosphorylation. Two sharp peaks of S19 phosphorylation were detected at 1 and 3 min with approximately a 130% increase in phosphorylation for each peak. In addition there was a third broad peak beginning at 6 min after EGF stimulation with approximately a 150% increase in the extent of phosphate incorporation. Notably, the early peaks of RLC phosphorylation precede the first peaks of myosin-IIA (1.5 min) and myosin-IIB (2 min) assembly, whereas the late peak of S19 phosphorylation is coincident with the second peaks of myosin-IIA and myosin-IIB assembly.

To correlate the kinetics of myosin-II assembly with subcellular distribution, we examined the localization of the endogenous myosin II isoforms in MDA-MB-231 cells under normal growth conditions (Figure 2A). Both myosin-IIA and myosin-IIB showed a diffuse distribution throughout the cytoplasm and colocalized along stress fibers in the central region of the cell (Figure 2Ac). Myosin-IIA was enriched in cellular protrusions (Figure 2A, arrows), whereas very little myosin-IIB staining was observed in the cell periphery. Next we investigated the effect of EGF stimulation on myosin-II localization (Figure 2B). In unstimulated cells (time 0), both myosin-IIA and myosin-IIB were mostly cytoplasmic; however, myosin-IIB was excluded from the cell periphery of unstimulated cells. At 2 min after EGF stimulation, which corresponds to the first peak of myosin-IIA and myosin-IIB assembly, we detected prominent cortical localization of myosin-IIA (Figure 2C, arrowheads). Cortical localization of myosin-IIB was observed primarily in cell regions not undergoing active protrusion along with myosin-IIA (Figure 2C, arrows). Six minutes after EGF stimulation, which corresponds to the second peak of myosin-IIA assembly and also encompasses the second, broader peak of myosin-IIB assembly, prominent stress fibers could be observed for both myosin-IIA and myosin-IIB with some localization at the cell cortex (Figure 2B, arrows). Myosin-IIA and myosin-IIB enrichment in stress fibers was still visible after 10 min of stimulation, but by 20 min both myosin-IIA and myosin-IIB redistributed to the cytoplasm with a reduction in stress fiber staining.

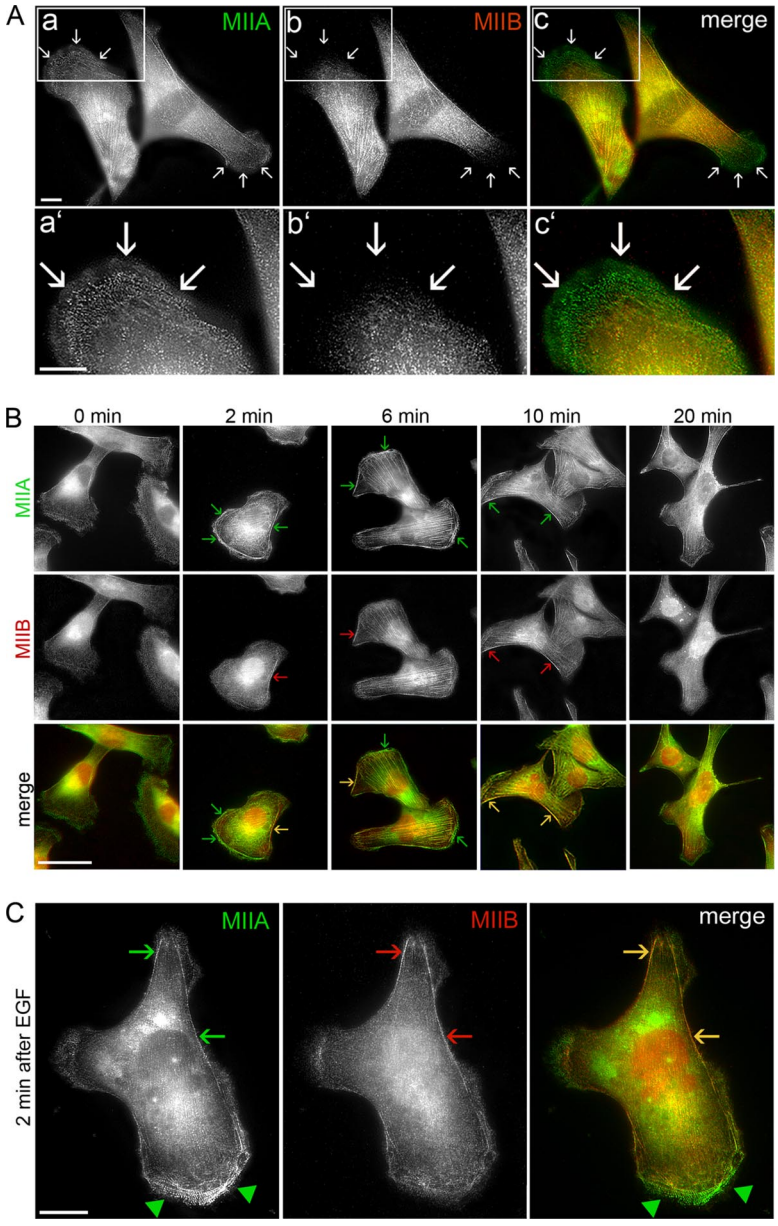


**Figure 2.** Localization of the endogenous myosin II isoforms in MDA-MB-231 cells. (A) Cells in normal growth medium. Myosin IIA (a and a′) and myosin IIB (b and b′) were detected by direct immunofluorescence using isoform-specific polyclonal antibodies. (c and c′) An overlay of the two images. Arrows indicate cell protrusions. Bar, 10 $\mu$m. (B) Localization of myosin-IIA and myosin-IIB in EGF-stimulated MDA-MB-231 cells. Arrows indicate cortical structures Bar, 50 $\mu$m. (C) Localization of myosin-IIA and myosin-IIB 2 min after EGF stimulation in MDA-MB-231 cells. Bar, 10 $\mu$m. Arrowheads and arrows indicate cellular regions undergoing active protrusions and regions not actively extending, respectively.

### *Cytosolic Myosin-IIA is Phosphorylated on the Heavy and Light Chains*

The occurrence of NMHC-IIB phosphorylation and its role in modulating assembly in vivo is well-documented (Ben-Ya'acov and Ravid, 2003; Even-Faitelson and Ravid, 2006; Rosenberg and Ravid, 2006). The in vivo consequences of NMHC-IIA phosphorylation have not been examined; therefore we focused our investigations on this isoform. At the peak of myosin-IIA heavy-chain phosphorylation (2–3 min after EGF stimulation), we observed a significant reduction in myosin-IIA associated with the Triton-insoluble fraction (Figure 1, A and B), suggesting that heavy-chain phosphorylation may mediate release of myosin-IIA from the cytoskeleton. In addition to phosphorylation on the heavy-chain, cytosolic myosin-IIA is also phosphorylated on the RLC at Thr-18 and Ser-19 (Figure 3, A and B). An examination of the stoichiometry of phosphorylation of the heavy chain in myosin-IIA immunoprecipitates showed that in unstimulated cells (0 min) the phosphate content was 0.45 mol phosphate per mol NMHC-IIA polypeptide chain. By 3 min after EGF stimulation, the phosphate content increased to 0.59 mol phosphate per mol NMHC-IIA polypeptide chain, which is consistent with the ~35% increase in phosphate content observed in our temporal assays (Figure 1B). Interestingly the phosphate content of the RLC did not change with 0.16 and 0.18 mol phosphate per mol RLC at 0 and 3 min, respectively.

### *In EGF-stimulated Cells the NMHC-IIA Is Phosphorylated on the CK2 Site*

To extend our findings regarding the phosphorylation status of the NMHC-IIA in EGF-stimulated cells, we performed phosphoamino acid analysis and phosphopeptide mapping studies on in vivo–phosphorylated myosin-IIA immunoprecipitated from MDA-MB-231 cells. Phosphoamino acid analysis of the NMHC-IIA revealed phosphorylation only on serine residues (Figure 4B). The NMHC-IIA phosphorylation sites were mapped by comparing phosphopeptide maps

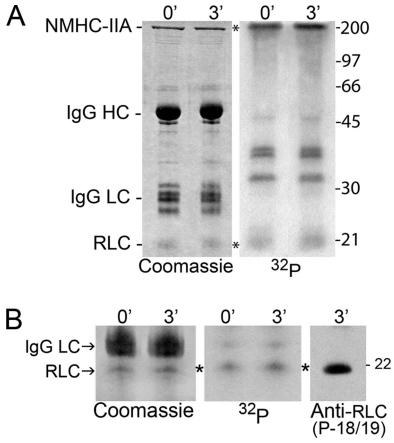


**Figure 3.** Myosin-IIA is phosphorylated on both the heavy and light chains. (A) Left, Coomassie-stained gel of myosin-IIA immunoprecipitates from unstimulated cells and cells 3 min after EGF stimulation. Right, corresponding autoradiogram. (B) Immunoblot of 3-min immunoprecipitate with a P-T18/S19 RLC antibody. Left, Coomassie-stained gel; middle, corresponding autoradiogram; right, immunoblot with P-T18/S19 antibody. The migration positions of the myosin-IIA heavy chain and RLC, and IgG heavy and light chains are indicated.

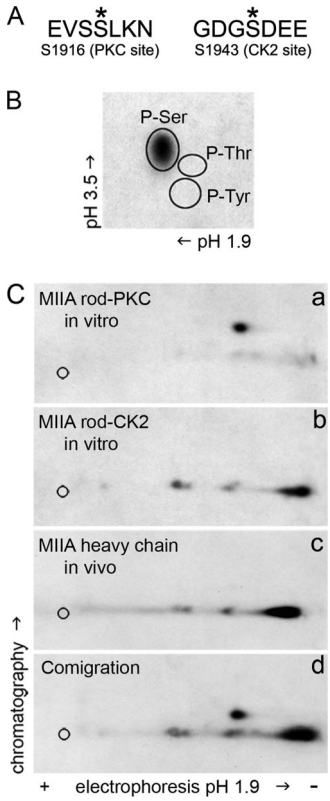


**Figure 4.** The myosin-IIA heavy chain is phosphorylated in vivo on serine residues at the CK2 site. (A) In vitro sites of NMHC-IIA phosphorylation. Myosin-IIA is phosphorylated on Ser-1916 near the C-terminal end of the α-helical coiled coil by PKC and on Ser-1943 in the tailpiece by CK2. (B) Phosphoamino acid analysis of the myosin-IIA heavy chain immunoprecipitated from EGF-stimulated cells showed that the heavy chain is phosphorylated on serine residues. Circles indicate the positions of phosphoamino acid standards. (C) Two-dimensional tryptic phosphopeptide maps of the myosin-IIA rod phosphorylated in vitro by (a) PKC alpha or (b) CK2, (c) endogenous myosin-IIA heavy chain from EGF-stimulated cells, and (d) mixture of in vitro– and in vivo–derived phosphopeptides. Based on the comigration of phosphopeptides from the CK2-phosphorylated myosin-IIA rod, the myosin-IIA heavy chain is phosphorylated in vivo on the CK2 site after EGF stimulation.

of the endogenous in vivo phosphorylated myosin-IIA heavy chain and recombinant myosin-IIA rods phosphorylated in vitro by PKC$\alpha$ or CK2 (Figure 4C). Phosphopeptide maps of in vitro–phosphorylated myosin-IIA rods showed one major PKC phosphopeptide and one major and two minor CK2 phosphopeptides (Figure 4C, a and b). The phosphopeptide map of the in vivo phosphorylated NMHC-IIA had a migration pattern that was identical to the phosphopeptide map of the CK2 phosphorylated myosin-IIA rod (Figure 4C, c). In addition, a phosphopeptide map of mixtures of the in vivo– and in vitro–derived phosphopeptides demonstrated that the phosphopeptides from the endogenous myosin-IIA comigrate with the CK2 phosphopeptides (Figure 4C, d). These observations indicate that the NMHC-IIA is phosphorylated on the CK2 site after EGF stimulation.

### *After EGF Stimulation, the Endogenous CK2 Associates with Myosin-IIA Rods*

We utilized a pulldown assay to evaluate whether CK2 associates with myosin-IIA in EGF-stimulated cells. $Ni^{2+}$-agarose containing bound, purified His-tagged myosin-IIA rods was incubated with the whole cell lysates from unstimulated or EGF-stimulated MDA-MB-231 cells (3 min). Protein complexes were evaluated by immunoblotting with an antibody against CK2$\alpha$. In unstimulated cells, very little CK2 was associated with the myosin-IIA rod (Figure 5, left panel). However the amount of CK2 that coprecipitated with the myosin-IIA rod increased considerably upon EGF stimulation (Figure 5, right panel). These results suggest a role for CK2 in mediating phosphorylation of the myosin-IIA heavy chain in response to EGF stimulation.

### *Biochemical Characterization and Cellular Localization of Myosin-IIA CK2 Phosphorylation Site (S1943) Mutants*

To examine the biological significance of heavy-chain phosphorylation on Ser-1943, first we evaluated the assembly properties of myosin-IIA S1943 mutants and the effect of S1943 substitutions on the interaction with S100A4. For these studies we utilized purified myosin-IIA rods containing alanine, aspartic, or glutamic acid substitutions at the CK2 phosphorylation site (S1943) to mimic constitutively phosphorylated or nonphosphorylated NMHC-IIA. Our previous studies demonstrated that stoichiometric phosphorylation of the heavy chain by CK2 reduces the assembly of myosin-IIA, in the presence of magnesium and 150 mM NaCl only 35% of the CK2-phosphorylated rods assemble (Dulyaninova *et al.*, 2005). Similarly, ~35% of the S1943D

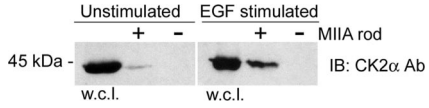


**Figure 5.** CK2 associates with myosin-IIA in response to EGF stimulation. The endogenous CK2 displayed increased association with His-tagged myosin-IIA rods in EGF-stimulated cells (3 min) compared with unstimulated cells. The $Ni^{2+}$-resin alone did not pull down CK2 from the whole cell lysates (w.c.l.). Protein complexes were detected by immunoblot with antibody against CK2 alpha subunits. Five percent of the whole cell lysate was run on the gel.

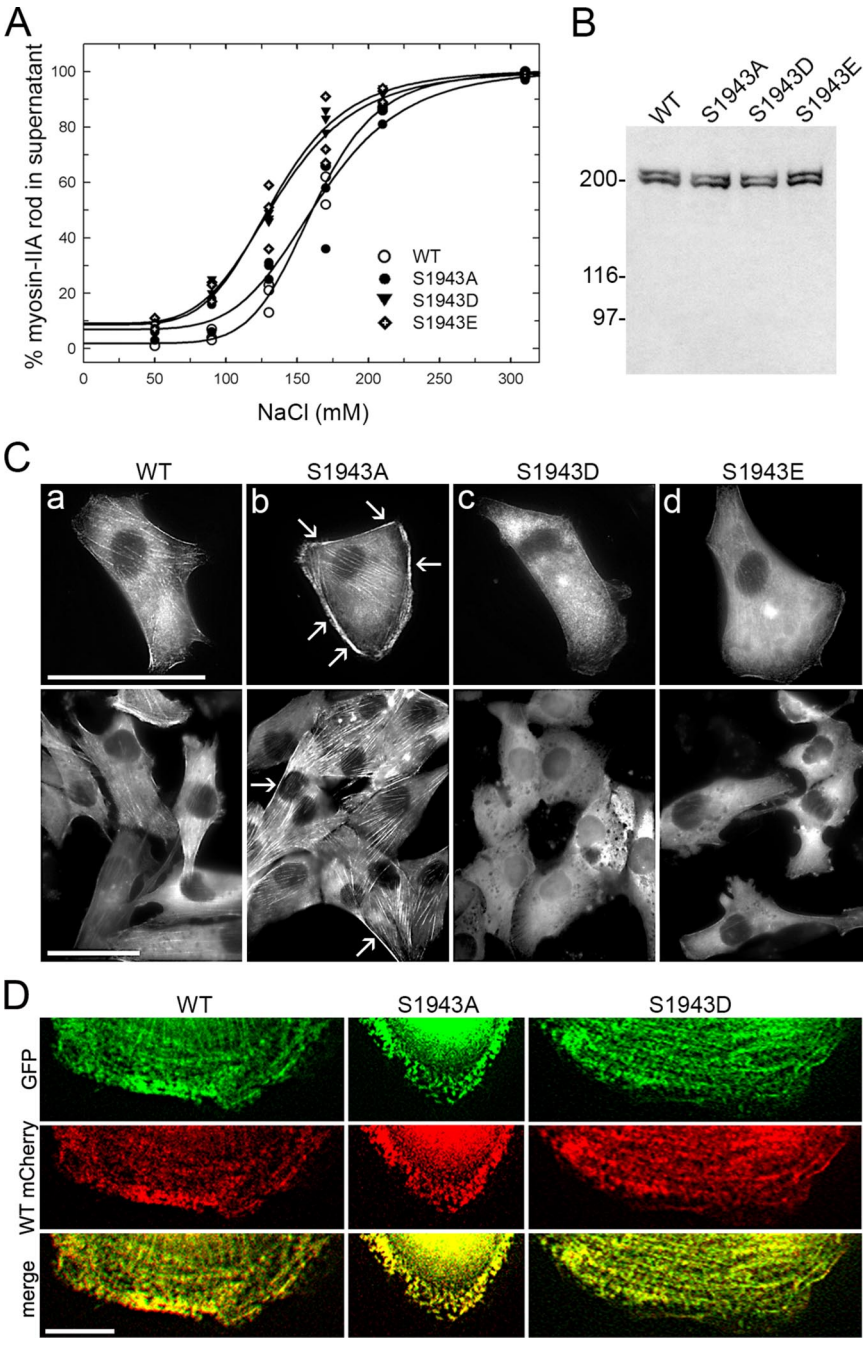


**Figure 6.** Biochemical characterization and cellular localization of the myosin-IIA CK2 site (S1943) mutants. (A) The assembly properties of wild-type, S1943A, S1943D, and S1943E myosin-IIA rods were monitored in a standard sedimentation assay. The assembly of the S1943D or E myosin-IIA rods was comparable to those of CK2-phosphorylated rods, whereas the S1943A rod assembled similarly to wild-type, unphosphorylated rods. ○, unphosphorylated myosin-IIA rods; ●, S1943A myosin-IIA rods; ▲, S1943D myosin-IIA rods; and ◇, S1943E myosin-IIA rods. The solid lines represent the best fit to the Hill equation. (B) Detection of full-length GFP-NMHC-IIA in MDA-MB-231 cells. Whole cell lysates from stable transfectants were subjected to immunoblot analysis with an antibody against the C-terminus of the myosin-IIA heavy chain. The lower bands represent the endogenous myosin-IIA. (C) Distribution of GFP-NMHC-IIA constructs was visualized by green fluorescence in transient (top) or stable (bottom) transfectants in normal growth medium. The wild-type NMHC-IIA displayed both cytoplasmic and stress fiber localization. The S1943A NMHC-IIA demonstrated increased assembly as evidenced by the prominent stress fibers and strong cortical localization (arrows). The S1943E and S1943D NMHC-IIA were primarily cytoplasmic with minor assembly into stress fibers and the cell cortex. Bar, 50 $\mu$m. (D) Wild-type mCherry-NMHC-IIA colocalizes with wild-type, S1943A, or S1943D GFP-NMHC-IIA in EGF-stimulated cells. Transient transfectants were fixed 4–6 min after EGF stimulation. Both S1943A and S1943D GFP-NMHC-IIA form puncta, which localize with wild-type mCherry-NMHC-IIA puncta in extending lamellae. Bar, 10 $\mu$m.

and S1943E myosin-IIA rods assemble at 150 mM NaCl (Figure 6A). A comparison of the midpoints shows that the assembly of the S1943D/E rods is more sensitive to the NaCl concentration than wild-type unphosphorylated and the S1943A myosin-IIA rods (Table 1, Figure 6A). Moreover, the midpoints of assembly for the S1943D/E rods are comparable to the midpoint of assembly for CK2-phosphorylated rods (126.4 ± 3.8 mM NaCl; Dulyaninova *et al.*, 2005). Thus, substitution of S1943 with aspartic or glutamic acid affects myosin-IIA assembly in a similar manner as CK2 phosphorylation.

We also examined the effects of the S1943 substitutions on the equilibrium binding of S100A4 in a cosedimentation assay, because CK2 phosphorylation of the myosin-IIA heavy chain significantly inhibited S100A4 binding ($K_d$ = ~22 $\mu$M; Dulyaninova *et al.*, 2005). Interestingly substitution of S1943 with aspartic or glutamic acid did not affect S100A4

**Table 1.** Effect of S1943 substitutions on myosin-IIA rod assembly

| Myosin-IIA rod construct | Midpoint (mM) |
|---|---|
| Unphosphorylated | 161.5 ± 1.9 |
| S1943A | 165.4 ± 5.3 |
| S1943D | 129.5 ± 2.3 |
| S1943E | 136.5 ± 4.9 |

Values represent the mean ± SD for three independent experiments.

**Table 2.** Effect of S1943 substitutions on S100A4 binding

| Myosin-IIA rod construct | $K_d$ ($\mu$M) |
|---|---|
| Unphosphorylated | 4.8 ± 0.9 |
| S1943A | 5.4 ± 1.0 |
| S1943D | 4.7 ± 1.0 |
| S1943E | 5.1 ± 1.0 |

Values represent the mean ± SEM for three to six independent experiments.

binding to the myosin-IIA rod (Table 2), indicating that charge replacement of the phosphorylatable serine does not mimic all aspects of heavy-chain phosphorylation at the CK2 site.

For in vivo studies, full-length, GFP-tagged NMHC-IIA constructs containing alanine, aspartic, or glutamic acid substitutions at the CK2 site were created as well. We expressed GFP-NMHC-IIA CK2 site mutants in MDA-MB-231 cells to analyze the effects of the S1943 substitutions on the myosin-IIA distribution in fixed cells. Immunoblot analysis with an antibody against the C-terminal 12 residues of the NMHC-IIA confirmed the expression of the full-length wild-type or S1943 mutant GFP-NMHC-IIA constructs in MDA-MB-231 cells and showed that they are expressed at comparable levels to the endogenous NMHC-IIA (Figure 6B). The distribution of the GFP-NMHC-IIA constructs in asynchronously growing cells was visualized by green fluorescence (Figure 6C). The localization of the wild-type GFP-NMHC-IIA was similar to the endogenous myosin-IIA (compare Figures 2A and 6C). The S1943E and S1943D GFP-NMHC-IIA showed a primarily cytoplasmic distribution with little stress fiber or cortical localization. In contrast, substitution of S1943 with alanine resulted in increased stress fibers and prominent cortical localization (Figure 6C, arrows). In EGF-stimulated cells, both the S1943A and S1943D GFP-NMHC-IIA form puncta in extending protrusions, suggesting that the alanine and aspartic acid substituted constructs can form filaments. In cells cotransfected with wild-type mCherry-NMHC-IIA and either wild-type, S1943A or S1943D GFP-NMHC-IIA, we observed a high degree of overlap between the two signals (Pearson's coefficient of 0.87 ± 0.06 for wild-type, 0.91 ± 0.07 for S1943A, and 0.93 ± 0.09 for S1943D), suggesting coassembly of wild-type and S1943A or S1943D NMHC-IIA in vivo.

### *The Phosphorylation Status of the CK2 Site Regulates Directional Migration*

To examine the effects S1943 substitutions on cell motility, we determined the ability of cells stably expressing GFP-NMHC-IIA constructs to cover a wound. Six independent experiments were performed for each cell line and a typical example is shown in Figure 7A. Cells expressing the wild-type GFP-NMHC-IIA migrated and covered the gap within 30 h, whereas cells expressing the S1943E or S1943D GFP-NMHC-IIA covered this area in ~24 h. For cells expressing the S1943A GFP-NMHC-IIA, a reduced rate of wound closure was observed with only ~70% of the open area covered by the cells in a 24-h period. Quantification of wound-induced migration during the first 4 h of wound healing showed that the rate of migration for S1943D/E GFP-NMHC-IIA–expressing cells increased about twofold (40 ± 3 and 33 ± 3 $\mu$m/h) compared with untransfected (21 ± 2 $\mu$m/h) or wild-type–expressing cells (22 ± 3 $\mu$m/h; Figure 7B). Cells expressing the S1943A GFP-NMHC-IIA exhibited approximately a twofold reduction in the rate of migration (12 ± 2 $\mu$m/h).

### *Increased Assembly of Myosin-IIA Promotes More Stable Focal Adhesions*

Because myosin-II functions in the formation of focal adhesions (Chrzanowska-Wodnicka and Burridge, 1996; Conti *et al.*, 2004), we examined focal adhesions by immunofluorescence with a paxillin pY118 antibody in EGF-stimulated cells. Before EGF stimulation (time 0), untransfected MDA-MB-231 cells contain numerous mature focal contacts (Figure 8A). By 2 min after EGF stimulation, the paxillin pY118 phosphotyrosine staining became more diffuse and dispersed. At 2–6 min after EGF addition, small, new focal contacts were visible in lamellae, which continued to in-

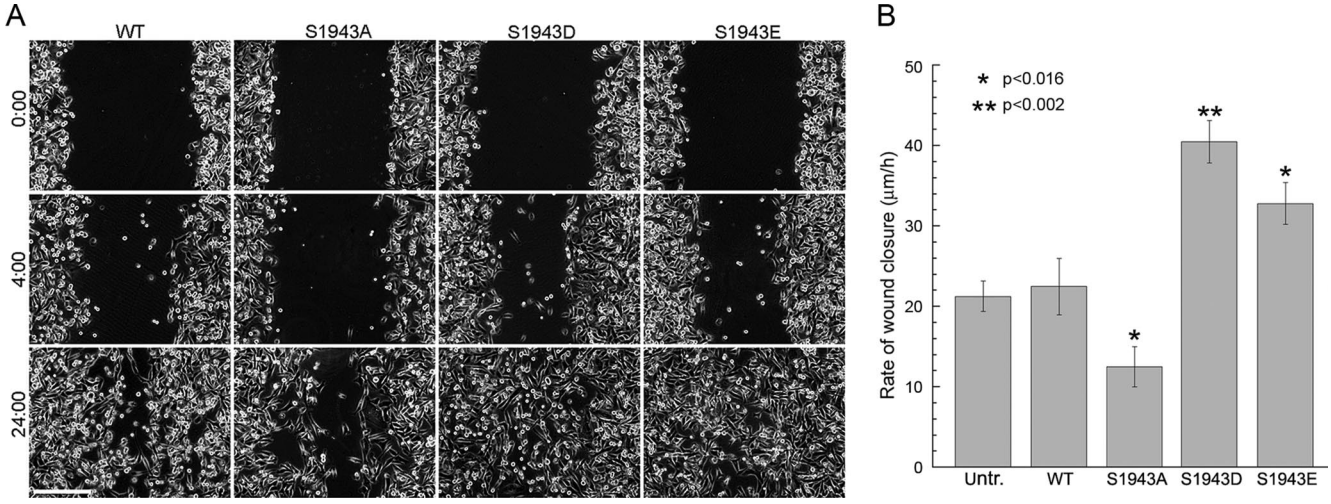


**Figure 7.** Expression of myosin-IIA S1943 mutants affects cell migration in a wound-healing assay. (A) Confluent monolayers of untransfected or stable MDA-MB-231 transfectants expressing either wild-type GFP-NMHC-IIA or S1943 mutants were wounded at time 0. Bar, 250 $\mu$m. (B) The average rate of wound closure during the first 4 h of wound healing was calculated from three independent experiments. Values represent the mean ± SD. Asterisk (*) denotes a statistically significant difference compared with wild-type GFP-NMHC-IIA cells.

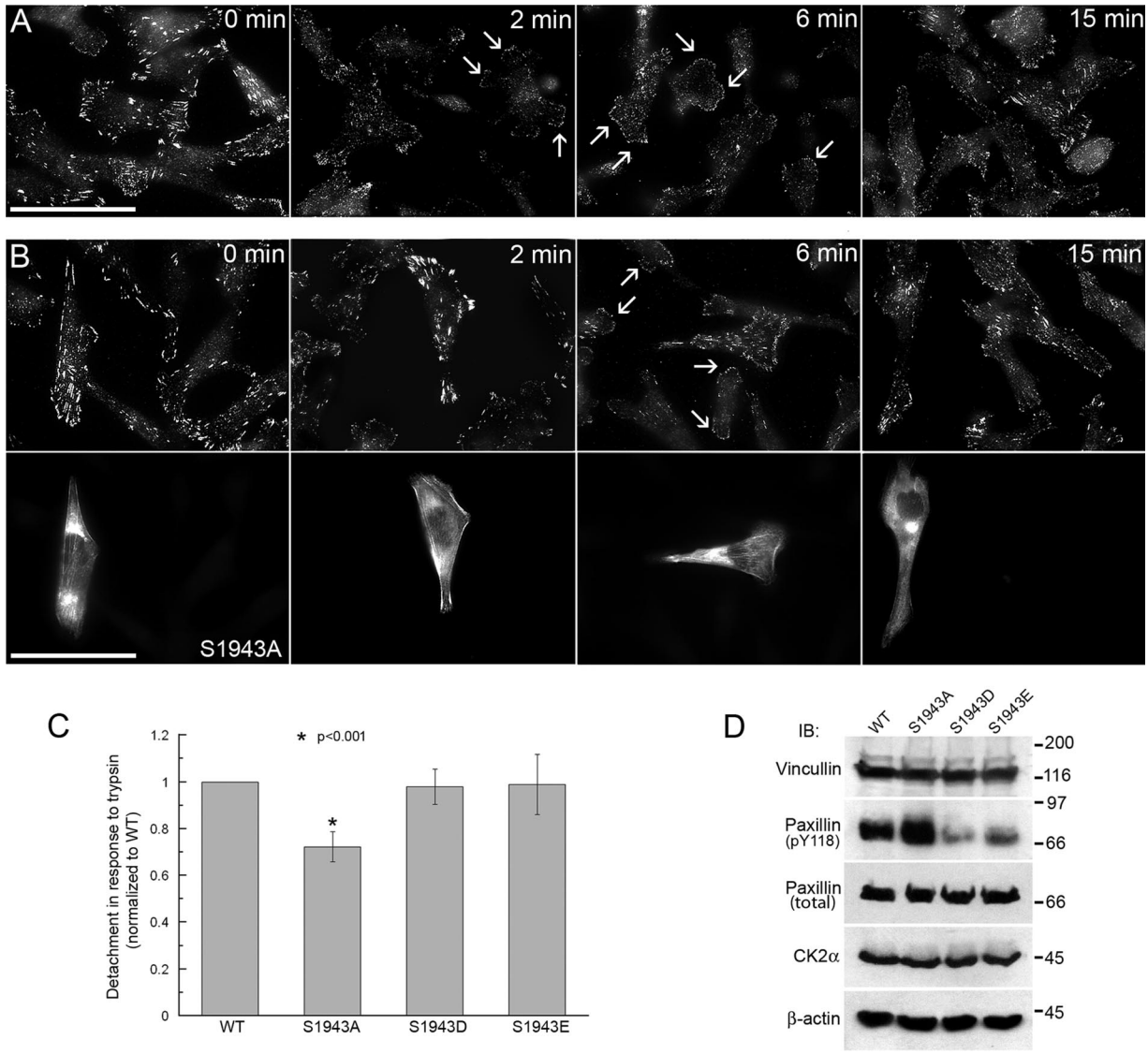


**Figure 8.** Stable focal adhesions are observed in GFP-NMHC-IIA S1943A–expressing cells. (A) Dynamic alteration of focal adhesions is observed in response to EGF stimulation in untransfected MDA-MB-231 cells by immunostaining with a paxillin pY118 phosphotyrosine antibody. (B) In transient transfectants expressing the GFP-NMHC-IIA S1943A, EGF-stimulated destabilization of pre-existing focal adhesions due to removal of phosphotyrosine is inhibited. Top, paxillin pY118 phosphotyrosine immunostaining; bottom, GFP fluorescence. Arrows indicate small, new focal contacts that are visible in the extending lamellae of untransfected cells. Bar, 50 $\mu$m. (C) Cell detachment assay on MDA-MB-231 cells stably expressing GFP-NMHC-IIA S1943 mutants. Adhesion was determined by calculating the percentage of total cells that detached in response to trypsin treatment. Expression of the GFP-NMHC-IIA S1943A resulted in ~30% increase in resistance to detachment as compared with wild-type, S1943D- and S1943E-expressing cells. Asterisk (*) denotes a statistically significant difference compared with wild-type GFP-NMHC-IIA cells. (D) Immunoblots of GFP-NMHC-IIA stable transfectants 2 min after EGF addition with antibodies to vinculin, pY118 paxillin, total paxillin, CK2$\alpha$, or actin. Relative to cells expressing wild-type GFP-MHC-IIA, S1943A cells display increased pY118 paxillin incorporation, and S1943D/E cells show decreased phosphotyrosine content. The levels of vinculin and CK2 were not altered in the different transfectants. Actin was used as a loading control.

crease in size (Figure 8A, 6 and 15 min). The dissolution and formation of focal contacts in cells expressing either the GFP-NMHC-IIA S1943D or S1943E was similar to that observed in untransfected cells (data not shown). However, in cells expressing the GFP-NMHC-IIA S1943A large focal contacts were observed at 2 min after EGF addition, which persisted for up to 6 min (Figure 8B).

To examine the stability of focal adhesions in cells expressing the GFP-MHC-IIA constructs, we assessed the adhesion competence of the stable myosin-IIA transfectants in a cell detachment assay. Cells expressing the GFP-MHC-IIA S1943A were ~30% more resistant to detachment than wild type, S1943D- or S1943E-expressing cells (Figure 8C). To confirm that the increased adhesiveness of S1943A expressing cells correlates with elevated tyrosine phosphorylation of paxillin, we analyzed the paxillin phosphotyrosine content of EGF-stimulated MDA-MB-231 cell lysates (Figure 8D). When compared with cells expressing wild-type GFP-NMHC-IIA– or GFP-NMHC-IIA-S1943A–expressing cells contained elevated levels of pY118 paxillin. In addition, we observed reduced phosphotyrosine incorporation into paxillin in cells expressing either the GFP-NMHC-IIA S1943D or

S1943E. The levels of total paxillin, vinculin, and CK2 were not altered in the different transfectants.

### *Alterations in Myosin-IIA Assembly Affect EGF-mediated Lamellipod Extension*

To evaluate whether the alterations in wound healing induced migration exhibited by GFP-NMHC-IIA mutant-expressing cells are also observed when responding to a chemotactic stimulus, we examined lamellipod extension after bath application of EGF. Untransfected MDA-MB-231 cells responded typically by a global extension of lamella, which resulted in a 32% increase in cell area (Figure 9, A and B). Cells expressing the wild-type GFP-NMHC-IIA displayed a response that was similar to parental cells; however, GFP-NMHC-IIA S1943A–expressing cells exhibited minimal lamellipod extension, which resulted in a 14% increase in the initial cell area (Figure 9B). In contrast, cells expressing the S1943D/E mutants showed significantly enhanced extension, with total area increases of 61 and 52%, respectively.

## DISCUSSION

Results presented here demonstrate that EGF stimulation induces transient assembly and phosphorylation of NMHC-IIA and NMHC-IIB in human breast carcinoma cells. In accordance with data demonstrating that the NMHC-II isoforms have unique cellular functions, the kinetics of assembly and phosphorylation differ for the A and B isoforms. In addition, there are significant differences in the kinetics of RLC monophosphorylation (P-S19) and diphosphorylation (P-T18/P-S19). Our analyses show that RLC phosphorylation precedes or is coincident with the assembly of the two myosin-II isoforms, consistent with the idea that RLC phosphorylation promotes filament assembly.

With respect to NMHC-IIA, the peak of heavy-chain phosphorylation occurs temporally between the two peaks of myosin-IIA assembly. Localization studies indicate that the peaks of assembly correspond to different cellular distributions of myosin-IIA, with peak 1 associated with cortical structures and peak 2 associated with stress fibers. These observations suggest that NMHC-IIA phosphorylation may promote the release of myosin-IIA from cortical filaments, thus providing a mechanism for recycling of myosin-IIA monomers and the turnover of myosin-IIA filaments. The physiological relevance of NMHC-IIA phosphorylation is supported by the high levels of phosphorylation observed 3 min after EGF stimulation (0.59 mol phosphate per mol NMHC-IIA polypeptide chain). For cytosolic myosin-IIA, the RLC is phosphorylated as well, albeit at a lower stoichiometry than observed for the heavy chain (0.18 mol phosphate per mol RLC). This low stoichiometry is not entirely unexpected because our kinetic assays indicate that phosphate turnover on the RLC is rapid after EGF stimulation. At this time, it is unclear if concomitant RLC dephosphorylation and NMHC-IIA phosphorylation contribute to the release of myosin-IIA from the cytoskeleton since we cannot determine the phosphorylation status of the heavy and light chains within the same myosin-IIA molecule.

Phosphopeptide maps of the endogenous myosin-IIA from EGF-stimulated cells demonstrate that the heavy chain is phosphorylated on the CK2 site (S1943), which is located in the C-terminal tailpiece of the heavy chain (Murakami *et al.*, 1998). CK2 recognizes a minimal consensus sequence of S/T-X-X-D/E; however, additional acidic residues at positions −2 to + 7 are needed for efficient phosphorylation of substrates (Meggio *et al.*, 1994). The amino acid sequence surrounding the CK2 site on the NMHC-IIA (GDGpS-

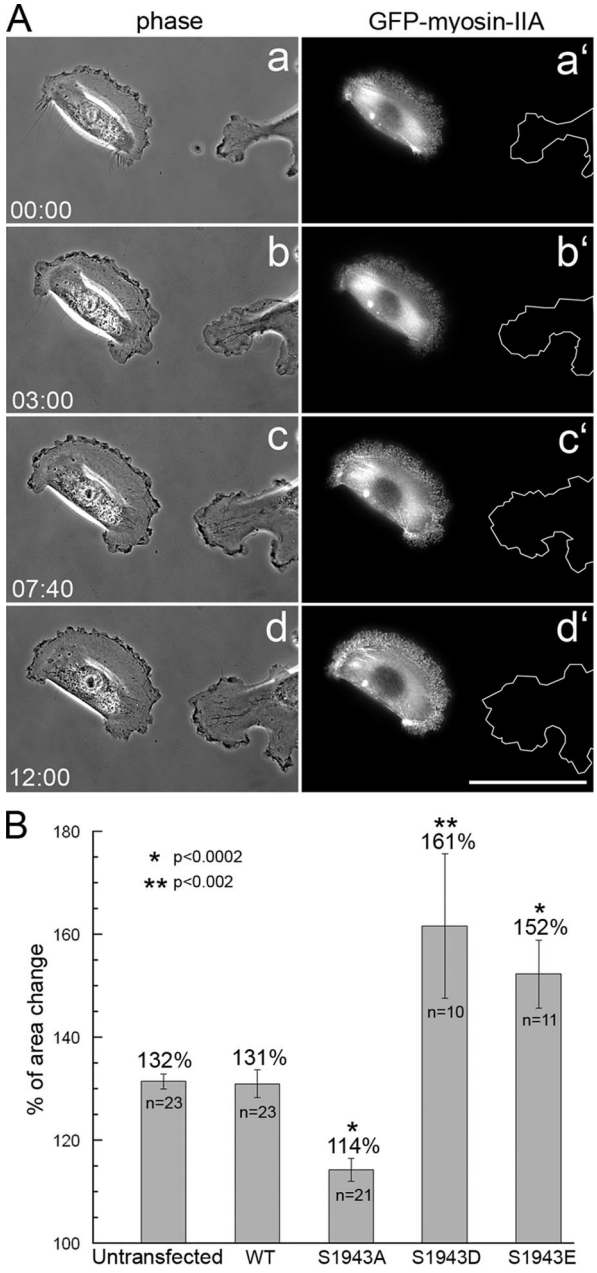


**Figure 9.** Expression of GFP-NMHC-IIA S1943 mutants affects EGF-induced lamellipod extension. MDA-MB-231 cells, parental or expressing the GFP-NMHC-IIA constructs, were stimulated with EGF and changes in cell shape were monitored by phase-contrast and fluorescence microscopy. (A) Representative phase-contrast (a–d) and fluorescent (a′–d′) micrographs of an untransfected cell and cell expressing wild-type GFP-NMHC-IIA responding to chemoattractant. The cells are shown before EGF stimulation (time 0) and at several times after EGF treatment. Cell trace in the fluorescence panel (a′–d′) demonstrates the extending edge of an untransfected cell. Bar, 50 $\mu$m. (B) Quantitation of the changes in cell shape at 15 min after EGF stimulation. Lamellipod extension of stable or transient transfectants was evaluated as the overall increase in the total area of the cells after EGF stimulation. The area before stimulation was set as 100%, and the relative area change was calculated as a percentage of the initial cell area. Error bar, SE. Asterisk (*) denotes a statistically significant difference as compared with untransfected cells.

DEEVD) is enriched in the acidic residues that are required for recognition by CK2. In addition, the observation that the NMHC-IIA is an in vitro substrate of CK2 (Murakami *et al.*, 1998; Dulyaninova *et al.*, 2005) and our finding that CK2 displays increased association with myosin-IIA in EGF-stimulated cells suggest that CK2 directly mediates phosphorylation of NMHC-IIA in growth factor–stimulated breast cancer cells.

We demonstrated previously that phosphorylation of myosin-IIA on S1943 reduces filament formation and regulates the binding of S100A4 (Dulyaninova *et al.*, 2005). In vitro assembly assays and in vivo expression studies demonstrated that the alanine, and aspartic/glutamic acid substitutions at this position mimic the assembly properties of nonphosphorylated and phosphorylated wild-type myosin-IIA, respectively. Thus with respect to filament assembly, the monoanionic side chains of aspartic and glutamic acid reproduce the function of the dianionic phosphate group at S1943. Interestingly, aspartic and glutamic acid substitutions do not inhibit S100A4 binding, demonstrating that the addition of a single charged residue does not fully mimic the spatial and charge contributions of a dianionic phosphate group at position 1943.

The studies presented here demonstrate that NMHC-IIA phosphorylation has pronounced effects on the motility of MDA-MB-231 cells. The expression of constitutively phosphorylated or nonphosphorylatable analogs of the NMHC-IIA has opposing effects on cell migration and growth factor–stimulated cell protrusion. Cells expressing NMHC-IIA S1943D or E displayed enhanced directional migration into a wound and cell protrusion, whereas cells expressing NMHC-IIA S1943A exhibited reduced migration and protrusion. Our studies indicate that NMHC-IIA S1943A and S1943D coassemble with wild-type NMHC-IIA. If heavy-chain phosphorylation regulates myosin-IIA filament turnover, then incorporation of NMHC-IIA S1943A monomers into filaments would reduce filament turnover, resulting in the formation stable filaments. Stable myosin-IIA filaments could allow for increased contractile force, augmented retrograde flow and reduced cell protrusion. Conversely, incorporation of NMHC-IIA S1943D or E monomers into filaments would be expected to reduce filament stability, and as a consequence, decreased contractility. This would inhibit retrograde flow and allow for enhanced cell protrusion.

Our findings are consistent with published studies demonstrating a role for myosin-II motor function in retrograde flow and the regulation of protrusion. For example, microinjection of NEM-inactivated myosin S1 fragments reduces F-actin flow and enhances the extension of growth cones in neurons (Lin *et al.*, 1996). Inhibition of myosin-II activity with protein kinase inhibitors attenuates F-actin flow in the cell center of sea urchin coelomocytes (Henson *et al.*, 1999) and in the lamella of epithelial cells (Gupton *et al.*, 2002), and treatment of neurons with blebbistatin significantly reduces F-actin retrograde flow and increases cell protrusion (Medeiros *et al.*, 2006). More recently, studies of spreading mouse embryonic fibroblasts have indicated that myosin-IIA, and not myosin-IIB, primarily regulates retrograde flow (Cai *et al.*, 2006). The studies presented here indicate that heavy-chain phosphorylation provides another regulatory mechanism for modulating contractile force during cell motility and protrusion.

In addition, our studies suggest that the phosphorylation status of the NMHC-IIA also impacts the turnover of focal adhesions. We detected more stable focal adhesions in cells expressing NMHC-IIA S1943A after EGF stimulation as evidenced by paxillin pY118 staining. This observation is consistent with previous studies showing that a reduction in cytoskeletal contractility induces the disassembly of focal adhesions (Chrzanowska-Wodnicka and Burridge, 1996). Although our analyses did not reveal any gross alterations in focal adhesions in cells expressing NMHC-IIA S1943D or E, we detected reduced Y118 phosphorylation of paxillin in these cells after EGF stimulation. These findings suggest that reduced myosin-IIA filament assembly or filament instability also affects focal adhesions either at the level of adhesion assembly or in their rate of turnover. Taken together, these studies support a direct role for NMHC-IIA phosphorylation in modulating myosin-IIA assembly during cell migration.

## ACKNOWLEDGMENTS

We thank Dr. Robert Adelstein and Dr. Thomas Egelhoff for the corrected full-length nonmuscle myosin-IIA construct. We are grateful to Dr. Thomas Meier for providing the CK2 antibody and Dr. Jonathon Backer for the use of his HTLE 7000 thin-layer electrophoresis unit. We also thank Anastasia Makris for excellent technical support. This work was supported by National Institutes of Health Grant GM069945.

## REFERENCES

Ben-Ya'acov, A., and Ravid, S. (2003). Epidermal growth factor-mediated transient phosphorylation and membrane localization of myosin II-B are required for efficient chemotaxis. J. Biol. Chem. *278*, 40032–40040.

Betapudi, V., Licate, L. S., and Egelhoff, T. T. (2006). Distinct roles of nonmuscle myosin II isoforms in the regulation of MDA-MB-231 breast cancer cell spreading and migration. Cancer Res. *66*, 4725–4733.

Bolte, S., and Cordelieres, F. P. (2006). A guided tour into subcellular colocalization analysis in light microscopy. J. Microsc. *224*, 213–232.

Bresnick, A. R. (1999). Molecular mechanisms of nonmuscle myosin-II regulation. Curr. Opin. Cell Biol. *11*, 26–33.

Brzeska, H., and Korn, E. D. (1996). Regulation of class I and class II myosins by heavy chain phosphorylation. J. Biol. Chem. *271*, 16983–16986.

Cai, Y. *et al.* (2006). Nonmuscle myosin IIA-dependent force inhibits cell spreading and drives F-actin flow. Biophys. J. *91*, 3907–3920.

Cashel, M., Lazzarini, R. A., and Kalbacher, B. (1969). An improved method for thin-layer chromatography of nucleotide mixtures containing $^{32}$P-labelled orthophosphate. J. Chromatogr. *40*, 103–109.

Chambers, A. F., Groom, A. C., and MacDonald, I. C. (2002). Dissemination and growth of cancer cells in metastatic sites. Nat. Rev. Cancer *2*, 563–572.

Chrzanowska-Wodnicka, M., and Burridge, K. (1996). Rho-stimulated contractility drives the formation of stress fibers and focal adhesions. J. Cell Biol. *133*, 1403–1415.

Clark, K., Langeslag, M., van Leeuwen, B., Ran, L., Ryazanov, A. G., Figdor, C. G., Moolenaar, W. H., Jalink, K., and van Leeuwen, F. N. (2006). TRPM7, a novel regulator of actomyosin contractility and cell adhesion. EMBO J. *25*, 290–301.

Conti, M. A., Even-Ram, S., Liu, C., Yamada, K. M., and Adelstein, R. S. (2004). Defects in cell adhesion and the visceral endoderm following ablation of nonmuscle myosin heavy chain II-A in mice. J. Biol. Chem. *279*, 41263–41266.

Conti, M. A., Sellers, J. R., Adelstein, R. S., and Elzinga, M. (1991). Identification of the serine residue phosphorylated by protein kinase C in vertebrate nonmuscle myosin heavy chains. Biochemistry *30*, 966–970.

Dulyaninova, N. G., Malashkevich, V. N., Almo, S. C., and Bresnick, A. R. (2005). Regulation of myosin-IIA assembly and Mts1 binding by heavy chain phosphorylation. Biochemistry *44*, 6867–6876.

Dulyaninova, N. G., Patskovsky, Y. V., and Bresnick, A. R. (2004). The N-terminus of the long MLCK induces a disruption in normal spindle morphology and a metaphase arrest. J. Cell Sci. *117*, 1481–1493.

Egelhoff, T. T., Lee, R. J., and Spudich, J. A. (1993). *Dictyostelium* myosin heavy chain phosphorylation sites regulate myosin filament assembly and localization in vivo. Cell *75*, 363–371.

Even-Faitelson, L., and Ravid, S. (2006). PAK1 and aPKCzeta regulate myosin II-B phosphorylation: a novel signaling pathway regulating filament assembly. Mol. Biol. Cell *17*, 2869–2881.

Garrett, S. C., Varney, K. M., Weber, D. J., and Bresnick, A. R. (2006). S100A4, a mediator of metastasis. J. Biol. Chem. *281*, 677–680.

Golomb, E., Ma, X., Jana, S. S., Preston, Y. A., Kawamoto, S., Shoham, N. G., Goldin, E., Conti, M. A., Sellers, J. R., and Adelstein, R. S. (2004). Identification and characterization of nonmuscle myosin II-C, a new member of the myosin II family. J. Biol. Chem. *279*, 2800–2808.

Gupton, S. L., Salmon, W. C., and Waterman-Storer, C. M. (2002). Converging populations of f-actin promote breakage of associated microtubules to spatially regulate microtubule turnover in migrating cells. Curr. Biol. *12*, 1891–1899.

Henson, J. H., Svitkina, T. M., Burns, A. R., Hughes, H. E., MacPartland, K. J., Nazarian, R., and Borisy, G. G. (1999). Two components of actin-based retrograde flow in sea urchin coelomocytes. Mol. Biol. Cell *10*, 4075–4090.

Huang, H., Paliouras, M., Rambaldi, I., Lasko, P., and Featherstone, M. (2003). Nonmuscle myosin promotes cytoplasmic localization of PBX. Mol. Cell. Biol. *23*, 3636–3645.

Hulme, E., and Birdsall, N. (1992). Receptor-Ligand Interactions. A Practical Approach, New York: IRL Press/Oxford University Press.

Jana, S. S., Kawamoto, S., and Adelstein, R. S. (2006). A specific isoform of nonmuscle myosin II-C is required for cytokinesis in a tumor cell line. J. Biol. Chem. *281*, 24662–24670.

Kolega, J. (1998). Cytoplasmic dynamics of myosin IIA and IIB: spatial 'sorting' of isoforms in locomoting cells. J. Cell Sci. *111*, 2085–2095.

Kolega, J. (2006). The role of myosin II motor activity in distributing myosin asymmetrically and coupling protrusive activity to cell translocation. Mol. Biol. Cell *17*, 4435–4445.

Kovacs, M., Wang, F., Hu, A., Zhang, Y., and Sellers, J. R. (2003). Functional divergence of human cytoplasmic myosin II: kinetic characterization of the non-muscle IIA isoform. J. Biol. Chem. *278*, 38132–38140.

Kriajevska, M. V., Cardenas, M. N., Grigorian, M. S., Ambartsumian, N. S., Georgiev, G. P., and Lukanidin, E. M. (1994). Non-muscle myosin heavy chain as a possible target for protein encoded by metastasis-related mts-1 gene. J. Biol. Chem. *269*, 19679–19682.

Laemmli, U. K. (1970). Cleavage of structural proteins during the assembly of the head of bacteriophage T4. Nature *227*, 680–685.

Li, Z.-H., and Bresnick, A. R. (2006). S100A4 regulates cellular motility via a direct interaction with myosin-IIA. Cancer Res. *66*, 5173–5180.

Li, Z.-H., Spektor, A., Varlamova, O., and Bresnick, A. R. (2003). Mts1 regulates the assembly of nonmuscle myosin-IIA. Biochemistry *42*, 14258–14266.

Lin, C. H., Espreafico, E. M., Mooseker, M. S., and Forscher, P. (1996). Myosin drives retrograde F-actin flow in neuronal growth cones. Neuron *16*, 769–782.

Litchfield, D. W., Dobrowolska, G., and Krebs, E. G. (1994). Regulation of casein kinase II by growth factors: a reevaluation. Cell. Mol. Biol. Res. *40*, 373–381.

Lo, C. M., Buxton, D. B., Chua, G. C., Dembo, M., Adelstein, R. S., and Wang, Y. L. (2004). Nonmuscle myosin IIb is involved in the guidance of fibroblast migration. Mol. Biol. Cell *15*, 982–989.

Maupin, P., Phillips, C. L., Adelstein, R. S., and Pollard, T. D. (1994). Differential localization of myosin-II isozymes in human cultured cells and blood cells. J. Cell Sci. *107*, 3077–3090.

Medeiros, N. A., Burnette, D. T., and Forscher, P. (2006). Myosin II functions in actin-bundle turnover in neuronal growth cones. Nat. Cell Biol. *8*, 215–226.

Meggio, F., Marin, O., and Pinna, L. A. (1994). Substrate specificity of protein kinase CK2. Cell. Mol. Biol. Res. *40*, 401–409.

Meshel, A. S., Wei, Q., Adelstein, R. S., and Sheetz, M. P. (2005). Basic mechanism of three-dimensional collagen fibre transport by fibroblasts. Nat. Cell Biol. *7*, 157–164.

Murakami, N., Chauhan, V. P., and Elzinga, M. (1998). Two nonmuscle myosin II heavy chain isoforms expressed in rabbit brains: filament forming properties, the effects of phosphorylation by protein kinase C and casein kinase II, and location of the phosphorylation sites. Biochemistry *37*, 1989–2003.

Murakami, N., Singh, S. S., Chauhan, V. P., and Elzinga, M. (1995). Phospholipid binding, phosphorylation by protein kinase C, and filament assembly of the COOH terminal heavy chain fragments of nonmuscle myosin II isoforms MIIA and MIIB. Biochemistry *34*, 16046–16055.

Obungu, V. H., Lee Burns, A., Agarwal, S. K., Chandrasekharapa, S. C., Adelstein, R. S., and Marx, S. J. (2003). Menin, a tumor suppressor, associates with nonmuscle myosin II-A heavy chain. Oncogene *22*, 6347–6358.

Rosenberg, M., and Ravid, S. (2006). Protein kinase Cgamma regulates myosin IIB phosphorylation, cellular localization, and filament assembly. Mol. Biol. Cell *17*, 1364–1374.

Rosenfeld, S. S., Xing, J., Chen, L. Q., and Sweeney, H. L. (2003). Myosin IIb is unconventionally conventional. J. Biol. Chem. *278*, 27449–27455.

Scholey, J. M., Taylor, K. A., and Kendrick-Jones, J. (1980). Regulation of non-muscle myosin assembly by calmodulin-dependent light chain kinase. Nature *287*, 233–235.

Segall, J. E., Tyerech, S., Boselli, L., Masseling, S., Helft, J., Chan, A., Jones, J., and Condeelis, J. (1996). EGF stimulates lamellipod extension in metastatic mammary adenocarcinoma cells by an actin-dependent mechanism. Clin. Exp. Metastasis *14*, 61–72.

Shaner, N. C., Campbell, R. E., Steinbach, P. A., Giepmans, B. N., Palmer, A. E., and Tsien, R. Y. (2004). Improved monomeric red, orange and yellow fluorescent proteins derived from *Discosoma* sp. red fluorescent protein. Nat. Biotechnol. *22*, 1567–1572.

Small, J. V. (1981). Organization of actin in the leading edge of cultured cells: influence of osmium tetroxide and dehydration on the ultrastructure of actin meshworks. J. Cell Biol. *91*, 695–705.

Straussman, R., Even, L., and Ravid, S. (2001). Myosin II heavy chain isoforms are phosphorylated in an EGF-dependent manner: involvement of protein kinase C. J. Cell Sci. *114*, 3047–3057.

Tullio, A. N., Accili, D., Ferrans, V. J., Yu, Z. X., Takeda, K., Grinberg, A., Westphal, H., Preston, Y. A., and Adelstein, R. S. (1997). Nonmuscle myosin II-B is required for normal development of the mouse heart. Proc. Natl. Acad. Sci. USA *94*, 12407–12412.

Vallely, K. M., Rustandi, R. R., Ellis, K. C., Varlamova, O., Bresnick, A. R., and Weber, D. J. (2002). Solution structure of human mts1 (S100A4) as determined by NMR spectroscopy. Biochemistry *41*, 12670–12680.

Wang, F., Kovacs, M., Hu, A., Limouze, J., Harvey, E. V., and Sellers, J. R. (2003). Kinetic mechanism of non-muscle myosin IIB: functional adaptations for tension generation and maintenance. J. Biol. Chem. *278*, 27439–27448.

Wei, Q., and Adelstein, R. S. (2000). Conditional expression of a truncated fragment of nonmuscle myosin II-A alters cell shape but not cytokinesis in HeLa cells. Mol. Biol. Cell *11*, 3617–3627.

Yamaguchi, H., Wyckoff, J., and Condeelis, J. (2005). Cell migration in tumors. Curr. Opin. Cell Biol. *17*, 559–564.